Ground motion model for median directional inelastic spectral displacements

Savvinos Aristeidou
PhD Candidate, Centre for Training and Research on Reduction of Seismic Risk (ROSE Centre), Scuola Universitaria Superiore IUSS Pavia, Pavia, Italy

Gerard J. O'Reilly
Assistant Professor, Centre for Training and Research on Reduction of Seismic Risk (ROSE Centre), Scuola Universitaria Superiore IUSS Pavia, Pavia, Italy

Karim Tarbali
Assistant Professor, University of Paris-Saclay, CentraleSupelec, Gif-sur-Yvette, France

ABSTRACT: Peak inelastic displacement of single-degree-of-freedom (SDOF) systems has been shown to be an efficient ground motion (GM) intensity measure (IM) for estimating the structural demand. Most ground motion models (GMMs) are developed to estimate the arbitrary or geometric mean of the two horizontal components of the response spectra obtained from the two orthogonal as-recorded directions of ground motion. Meanwhile, more recent GMMs have opted in estimating orientation-independent horizontal component definitions. This horizontal component definition has the advantage of removing the sensor orientation as a contributor to the estimated ground motion uncertainty. This is the definition adopted in this study, where the median directional inelastic spectral displacements were considered as an IM. To do this, a set of bilinear SDOF systems and a subset of the NGA-West2 database were used to fit a GMM to estimate the medians and dispersions of $Sd_{\mathrm{i,RotD50}}$ from shallow crustal earthquakes. These were calculated by rotating the ground motions through all non-redundant rotation angles in the horizontal plane. A set of functional forms was developed using the mixed-effects regression approach, with the predictor variables being the elastic vibration period, T, the force reduction factor, R, and a set of ground motion causal parameters. The results show how the model is able to predict the data quite well, while keeping the dispersions at a reasonable level.

1. INTRODUCTION

Selection of an appropriate ground motion (GM) intensity measure (IM) is of great importance for risk assessments. Empirical ground motion models (GMMs) provide the probability distributions for these IMs at a given site, caused by a specific earthquake event, needed for seismic hazard analyses, and allow the selection and scaling of representative GM records for non-linear response history analyses (NRHAs). The most common scalar IM currently used is the spectral acceleration *Sa* at a given vibration period T, $Sa(T)$. Since seismic shaking is felt principally in three dimensions, there is a need to consider the possible effects of ground motion directionality, which is illustrated graphically in Figure 1. As shown, different GMs may induce significantly different directional demands, depending both on the system and GM characteristics. Notably, Baker and Cornell (2006) addressed this question by discussing the regular use of an arbitrary *Sa* component, Sa_{arb}, or the geometric mean of the two as-recorded *Sa* components, Sa_{gm}, in probabilistic seismic analyses.

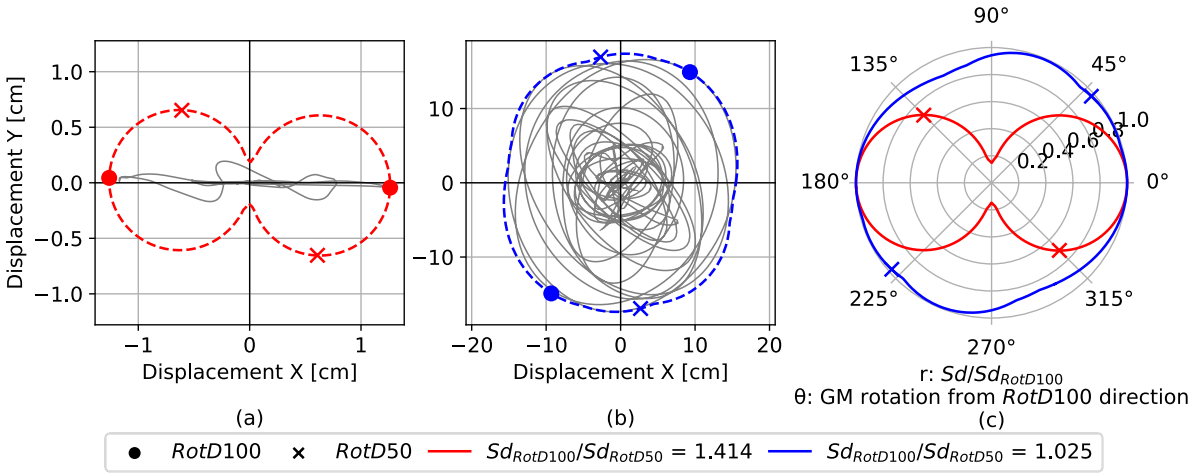

Figure 1: Trace response of an elastic SDOF oscillator with T = 2 s. (a) Strongly polarized GM; SMART1 O07 recording from the 1985 Taiwan SMART1(33) earthquake, RSN: 492. (b) Unpolarized GM; Dumbarton Bridge West End FF recording from the 1989 Loma Prieta earthquake, RSN: 757. (c) Polar plot of normalized spectral displacement in all horizontal directions for the two considered records in this figure.

In recent years, various horizontal component definitions have been proposed. Some of these definitions include the different percentiles of *Sa* over all non-redundant orientations (Boore 2010). Most recent GMMs have shifted towards these definitions of *Sa*, such as the Sa_{RotD50} (Campbell and Bozorgnia 2014). Boore (2010) defined the *RotDnn* component of *Sa* as the nn^{th} percentile of all rotation angles sorted by amplitude, with *D* denoting the period-dependent rotation angle. These *Sa* definitions (e.g., *RotD100* and *RotD50*) can be used to quantify the directional characteristics of GMs (Baker and Lee 2018; Tarbali 2017). In the same context, the NGA-West2 database (Ancheta et al. 2013) was used (Shahi and Baker 2014) to develop an empirical model for the $Sa_{\text{RotD100}}/Sa_{\text{RotD50}}$ ratio, which is the most common directionality (i.e., polarization) measure of horizontal ground motion pairs, as illustrated in Figure 1.

In addition to the issue of directionality, several studies have considered bidirectional or multi-directional excitation of either linear-elastic systems or complex non-linear structural systems (Pinzon et al. 2021; Roy et al. 2022). Several researchers have also developed GMMs for peak inelastic spectral displacements of SDOF systems, Sd_i, (Heresi et al. 2018; Huang et al. 2020; Stafford et al. 2016; Tothong and Cornell 2006). Under certain conditions, Sd_i has been demonstrated to be an effective IM to relate ground motion intensity and inelastic structural response (Luco and Cornell 2007).

In this study, the model of *RotDnn* for the 50^{th} percentile of Sd_i is presented for bilinear SDOF systems, with the 100^{th} percentile model presented in a more detailed journal paper (Aristeidou et al. 2023). The predictor variables are *T*, *R*, and a set of GM causal parameters described in Section 3.1.

In the following sections, the workflow followed is outlined, describing the GM database and the GMM functional forms used for the development of the model. This is then appraised via a performance assessment of the model and comparison with other models available in the literature.

2. METHODOLOGY

The methodology employed is outlined in Figure 2. First, the GMs within the range of M_w and R_{rup} of interest were extracted from the NGA-West2 database. Then, the range of *R* and *T* values, along with the hysteretic behavior, post-yield stiffness, and the damping of the SDOF system, were defined. For each SDOF system, the ground motions were rotated with an increment of 6° in

the range of 0° to 180° and applied to the numerical model developed in OpenSeesPy to obtain the peak displacements. The total number of analyses presented in this study amounted to 7139 GMs × 5 R × 13 T × 30 incidence angles to give 13,921,050 inelastic SDOF analyses.

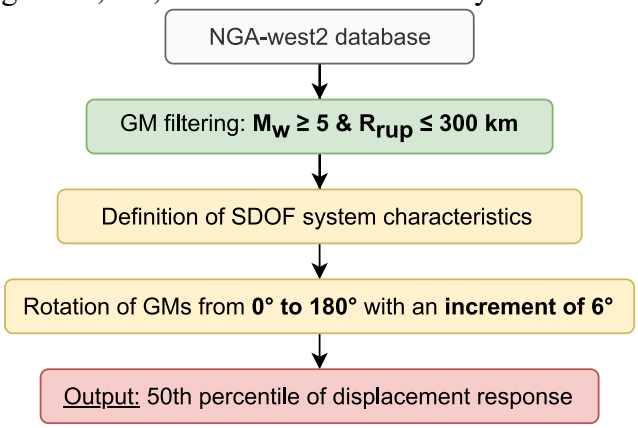

Figure 2: Illustration of the methodology adopted to generate data.

2.1. Strong motion database

The ground motion records used in this study were obtained from the NGA-West2 database (Ancheta et al. 2013). From this database, a subset of GMs recorded during earthquakes deemed of sufficient intensity to cause structural and/or non-structural damage was selected for the analyses. Specifically, the subset considered was ground motions with $M_w \geq 5$ and $R_{rup} \leq 300$ km. The scatter plot of the considered records in terms of M_w, R_{rup}, and $V_{s,30}$ is shown in Figure *3*. Additionally, GMs with maximum usable periods lower than the elastic period of the corresponding SDOF system in each case were filtered out of the considered GM subset.

2.2. Description of SDOF systems

The SDOF system chosen for this study was a bilinear model with a positive strain hardening ratio of α_s = 3%. The hysteretic behavior of this system is non-degrading and non-evolutionary. A tangent stiffness proportional damping model was adopted with a ratio of ξ = 5%. The set of elastic periods considered was T = 0.04, 0.06, 0.1, 0.2, 0.3, 0.5, 0.75, 1, 1.5, 2, 3, 4, 5 s, and the set of strength ratios was R = 1.5, 2, 3, 4, 6. The strength ratio, or force reduction factor, R, is defined as the ratio of maximum directional demand, $F_{el,RotD100}$, in the elastic system with period T subjected to a given ground motion, to the SDOF yield strength, F_y, computed by Eq. (1).

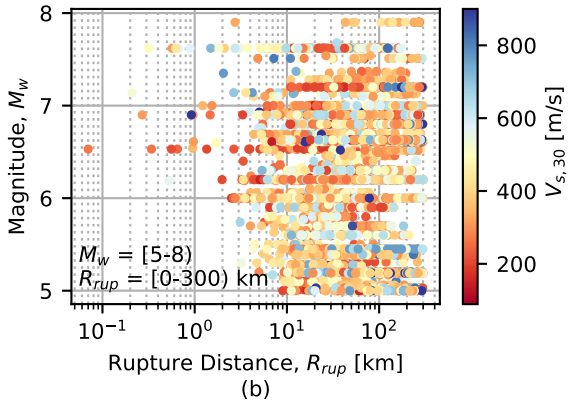

Figure 3: Distribution of the considered GMs in terms of M_w, R_{rup}, and $V_{s,30}$.

$$R = \frac{m \cdot Sa_{RotD100}}{F_y} \quad (1)$$

3. FITTING OF THE GROUND MOTION MODEL

3.1. Functional form

This section presents the developed model for the *RotD50* inelastic displacement demands. The main functional form of this model, which was chosen after many trial combinations of functional forms of existing GMMs examining the inelastic spectral displacement (Bozorgnia et al. 2010; Heresi et al. 2018; Huang et al. 2020), is given by:

$$\ln Y_{i,j} = a + F_M + F_D + F_{sof} + F_s + F_{basin} + \eta_i + \varepsilon_{i,j} \quad (2)$$

where, $Y_{i,j}$ is the 50^{th} percentile from all non-redundant incidence angles of peak inelastic spectral displacement demand $Sd_{i,RotD50}$ (in centimeters) at site j from event i; a is a model coefficient; F_M, F_D, F_{sof}, F_s, and F_{basin} are the magnitude scaling, distance function, style of faulting, site amplification, and the basin-effects correction terms, respectively. The model given in Eq. (2) separates the inter- and intra- event residuals (i.e., mixed-effects model). η_i is the inter-event residual corresponding to event i

following a normal distribution with zero mean and standard deviation τ; $\varepsilon_{i,j}$ is the intra-event residual corresponding to event i at station j following a normal distribution with zero mean and standard deviation φ. It should be noted that η_i and $\varepsilon_{i,j}$ are assumed to be mutually independent; therefore, the total standard deviation of the model is calculated as:

$$\sigma = \sqrt{\tau^2 + \varphi^2} \tag{3}$$

The magnitude function, which does not consider magnitude saturation, is given in Eq. (4):

$$F_M = b_1\left(M_{w,i} - M_r\right) + b_2\left(M_{w,i} - M_r\right)^2 \tag{4}$$

where, M_w is the moment magnitude, M_r is the reference magnitude taken here to be equal to 6, and b_1 and b_2 are model fitting coefficients. The distance function is:

$$F_D = \left[c_{1k} + c_{2k}\left(M_{w,i} - M_r\right)\right] \ln\left(\frac{R_{mod}}{R_{h2}}\right)$$

$$\begin{cases} k = 1; & R_{mod} \le R_{h1} \\ k = 2; & R_{h1} < R_{mod} \le R_{h2} \\ k = 3; & R_{mod} > R_{h2} \end{cases} \tag{5}$$

where R_{mod} is a modified distance to the source computed as:

$$R_{mod} = \sqrt{R_{rup}^2 + c_3^2} \tag{6}$$

where R_{rup} is the closest distance from the rupture plane to the site in km, c_3 is a model coefficient, and c_{1k} and c_{2k} are attenuation coefficients. R_{h1} and R_{h2} are hinge distances to account for the changes in the attenuation rate and are fixed to 15 and 150 km, respectively, and the index k is introduced to account for the different distance ranges. The style-of-faulting function is:

$$F_{sof} = f_1 F_{N,i} + f_2 F_{T,i}$$

$$\left(F_{N,i}, F_{T,i}\right) = \begin{cases} (0,0); & Strike - slip\ fault \\ (1,0); & Normal\ fault \\ (0,1); & Thrust\ fault \end{cases}$$

where, f_1 and f_2 are model fitting coefficients; F_N and F_T are binary variables representing the style of faulting. The site amplification function is:

$$F_s = s_n \cdot \ln\left(V_{s,30}\right)$$

$$\begin{cases} n = 1; & V_{s,30} < 400 \\ n = 2; & 400 \le V_{s,30} < 650 \\ n = 3; & 650 \le V_{s,30} < 1000 \\ n = 4; & V_{s,30} \ge 1000 \end{cases} \tag{8}$$

where, s_n is a model fitting coefficient with the index n differentiating between the different $V_{s,30}$ bins, where $V_{s,30}$ is in m/s. The basin-effects correction function is given as:

$$F_{basin} =$$

$$\begin{cases} d_1(Z_{2.5} - 1); & Z_{2.5} \le 1 \\ 0; & 1 < Z_{2.5} \le 3 \\ d_2\left[1 - e^{-0.25(Z_{2.5} - 3)}\right]; & Z_{2.5} > 3 \end{cases} \tag{9}$$

where, d_1 and d_2 are model fitting coefficients, and $Z_{2.5}$, is the depth to the 2.5 km/s shear-wave velocity horizon, typically referred to as basin or sediment depth in km. For the records without registered $Z_{2.5}$, the guidelines suggested in (Kaklamanos et al. 2011) were followed, utilizing the formulas given in (Abrahamson and Silva 2008; Campbell and Bozorgnia 2007) to estimate $Z_{2.5}$ from $V_{s,30}$.

The standard deviations τ and φ were computed through a series of iterative mixed-effects non-linear regressions (Abrahamson and Youngs 1992). Applying this regression procedure, the directions to find the resulting empirical coefficients and standard deviation values are indicated in Aristeidou et al. (2023).

3.2. GMM performance

To assess the performance of the model against the observed data, inspections on the prediction residuals were carried out. A residual here is defined as the difference between the 'observed empirical data' (i.e., the computed peak inelastic displacements according to the methodology shown in Figure 2) and the model prediction, both in natural logarithms. Thus, a positive residual indicates underprediction by the proposed model.

Figure 4 depicts the inter-event residuals versus the event magnitude for $Sd_{\text{i,RotD50}}$ and two different combinations of T and R. Plotted in the same figure are also the binned mean residual

values, ± one standard deviation. These results clearly indicate that the chosen functional form adequately represents the event term, as no apparent bias against M_w is observed. This trend was also observed across the entire range of T and R used in this study.

Figure 5 then shows the total residuals of the same cases with respect to R_{rup} for two different combinations of T and R. The observed lack of trend indicates that the functional form adopted is adequate for capturing the data trends.

Overall, the trends in Figure 4 and 5 hold true for the complete set of different SDOF systems considered. In addition, the predictive power of the GMM is also analyzed by comparing the observed and median predicted values of Sd_i for each system (i.e., different T and R), via the coefficient of determination R^2, which is observed to be around 0.8 for most of the cases.

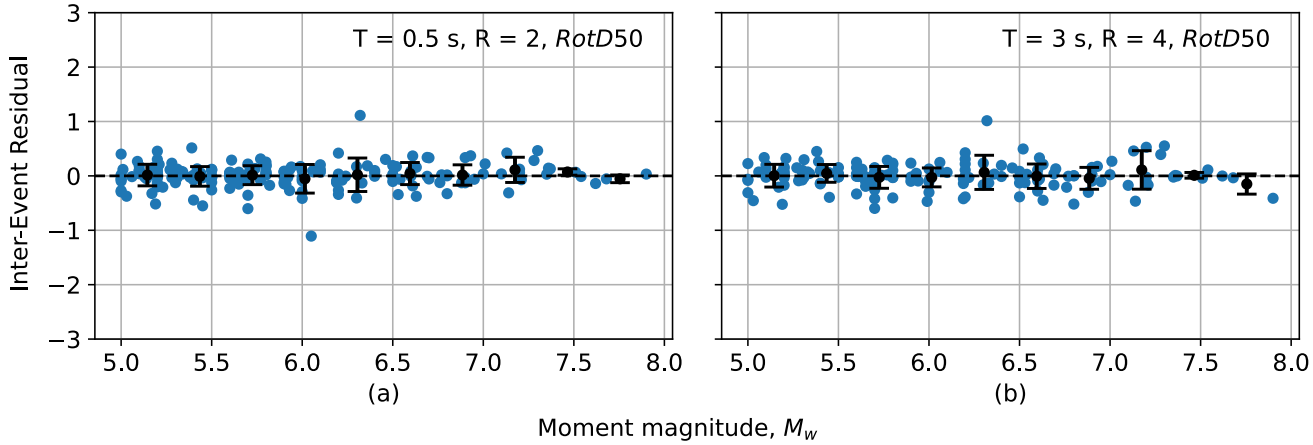

Figure 4: Inter-event residuals with respect to M_w for different T and R.

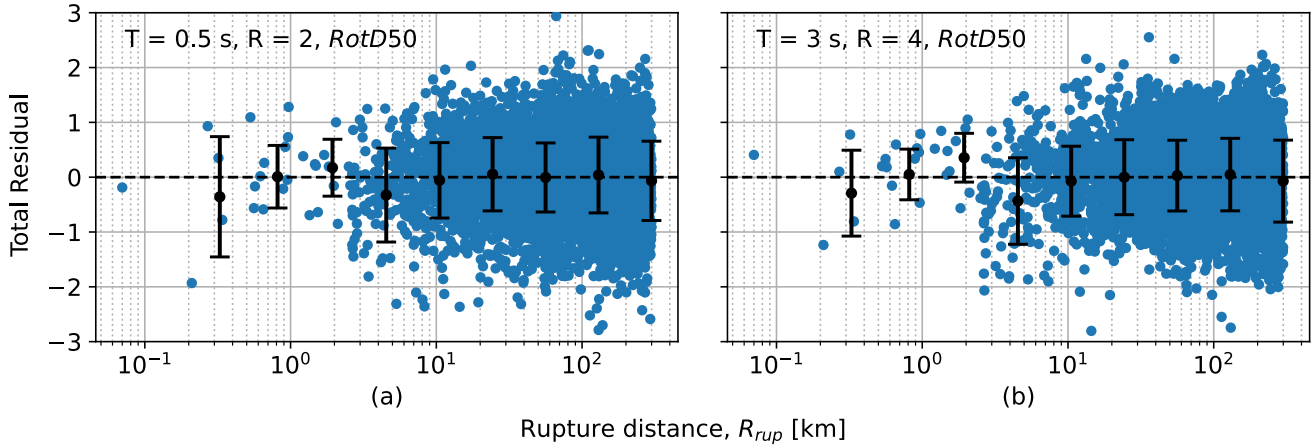

Figure 5: Total residuals with respect to R_{rup} for different T and R.

4. COMPARISON WITH PREVIOUS STUDIES

In conducting comparisons with the existing models, the difficulty was the fact that only a few available models quantified the inelastic displacement predictions in terms of the strength ratio R, instead they have used the ductility demand, μ, or the strength coefficient, C_y. Nonetheless, two models from the literature were used for comparison with the model proposed herein. Namely, the models proposed by Tothong and Cornell (2006) and Huang, Tarbali and Galasso (2020), denoted as TC06 and HTG20.

TC06 uses the outputs of a conventional (elastic) GMM and converts them to inelastic spectral displacements based on the proposed ratio model. Herein, the elastic GMM employed in the original paper was used (Abrahamson and Silva 1997), although in principle, any elastic GMM may be used. TC06 used 5% post-yield stiffness ratio, the maximum R_{rup} was limited to 95 km, and the arbitrary horizontal component, $Sd_{i,arb}$, was utilized for each recording. In HTG20, a region-specific GMM for inelastic spectral displacements was developed for northern Italy, explicitly accounting for the spatial correlation between intra-event residuals. The M_w range for HTG20 was from 4.0 to 6.4 and source-to-site distances less than 200 km. The geometric mean of the two horizontal components, $Sd_{i,gm}$, was utilized.

Two different comparisons are given in Figure 6 between the proposed GMM and the existing models from the literature. GMs were divided into distinct magnitude bins and compared with the median predicted values corresponding to the mean magnitude of GMs contained in each bin. It can be observed that the median prediction of the proposed GMM generally matches well the cloud median (shown via the dashed black lines) within the ranges containing a significant amount of data. More amplified differences are observed at large distances since the model does not explicitly account for anelastic attenuation effects and also at lower distances due to the data scarcity. The model of HTG20 is close to the proposed model for the lower magnitude bin but deviates a lot for $M_w > 7$. This is reasonable because of the aforementioned limited earthquake magnitude range of the HTG20 model. Meanwhile, the model of TC06 is quite close to the cloud median of the data, with the exception of overpredicting the displacements for large distances. Again it is important to highlight that these models were predicting different horizontal component definitions (i.e., $Sd_{i,arb}$ and $Sd_{i,gm}$) compared to the $Sd_{i,RotD50}$ being evaluated here.

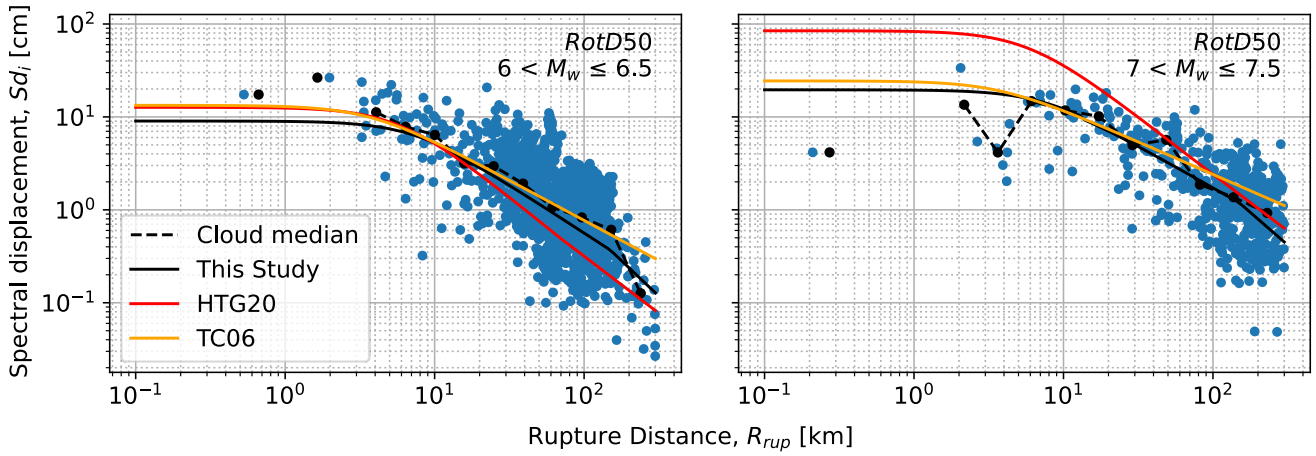

Figure 6: Median $Sd_{i,RotD50}$ predicted by the model, along with the empirical data, as a function of M_w and R_{rup}, for T = 1 s and R = 4.

5. GMM PREDICTION UNCERTAINTY

Figure 7 illustrates the total standard deviation of $\ln(Sd_{i,RotD50})$ and compares it with the corresponding values from the TC06 and HTG20 models. It can be observed that the model presented here gives lower standard deviations for most periods when comparted to TC06 and HTG20. This is partially explained by the different definitions of horizontal component. As shown in the literature (Beyer and Bommer 2006), using the *RotD50* component may reduce the dispersion in comparison to the arbitrary component used by TC06 and to the geometric mean used by HTG20. Noting that the reduction with respect to the geometric mean is minimal. In

HTG20 the difference in total standard deviation is primarily due to the difference in the intra-event standard deviation, which is a product of considering spatial correlation (Jayaram and Baker 2010).

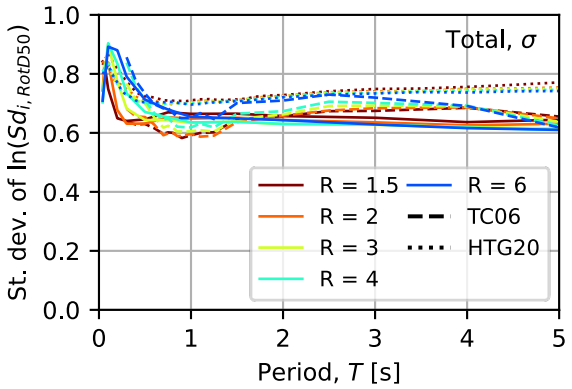

Figure 7: Total logarithmic standard deviation.

6. CONCLUSIONS

Based on the development of this model, the following can be noted:

- For what concerns the GMM developed to represent the *RotD50* horizontal component of inelastic spectral displacement demand, a mixed-effects regression model was fitted to the computed response quantities under ground motion recordings from shallow-crustal earthquakes.
- The proposed GMM exhibited reasonably low dispersions when compared with others available in the literature and is not sensitive to the level of non-linear demand.
- Compared to existing similar models, this GMM was fitted using a substantially large dataset of ground motions from the NGA-West2 database. It also does not require any auxiliary elastic GMM to predict the median and dispersion of inelastic displacements.
- The range of applicability of this GMM is the following: moment magnitude, $5 < M_w \leq 8$; rupture distance, $0 < R_{rup} \leq 300$ km; average shear-wave velocity in the top 30 m of the site profile, $90 \leq V_{s,30} \leq 1300$ m/s; period of vibration, $0.04 \leq T \leq 5$ s; strength ratio, $1 \leq R \leq 6$; tectonically active shallow crustal regions.

7. REFERENCES

Abrahamson, N. A., and W. J. Silva. 1997. "Empirical response spectral attenuation relations for shallow crustal earthquakes." *Seismol. Res. Lett.*, 68 (1): 94–109. https://doi.org/10.1785/gssrl.68.1.94.

Abrahamson, N. A., and R. R. Youngs. 1992. "A stable algorithm for regression analyses using the random effects model." *Bull. Seismol. Soc. Am.*, 82 (1): 505–510. https://doi.org/10.1785/BSSA0820010505.

Abrahamson, N., and W. Silva. 2008. "Summary of the Abrahamson & Silva NGA ground-motion relations." *Earthq. Spectra*, 24 (1): 67–97. https://doi.org/10.1193/1.2924360.

Ancheta, T., R. Darragh, J. Stewart, E. Seyhan, W. Silva, B. Chiou, K. Wooddell, R. Graves, A. Kottke, D. Boore, T. Kishida, and J. Donahue. 2013. "PEER NGA-West2 Database, Technical Report PEER 2013/03."

Aristeidou, S., K. Tarbali, and G. J. O'Reilly. 2023. "A Ground Motion Model for Orientation-Independent Inelastic Spectral Displacements from Shallow Crustal Earthquakes." (Under review): 1–23.

Baker, J. W., and C. A. Cornell. 2006. "Which spectral acceleration are you using?" *Earthq. Spectra*, 22 (2): 293–312. https://doi.org/10.1193/1.2191540.

Baker, J. W., and C. Lee. 2018. "An Improved Algorithm for Selecting Ground Motions to Match a Conditional Spectrum." *J. Earthq. Eng.*, 22 (4): 708–723. Taylor & Francis. https://doi.org/10.1080/13632469.2016.1264334.

Beyer, K., and J. J. Bommer. 2006. "Relationships between median values and between aleatory variabilities for different definitions of the horizontal component of motion." *Bull. Seismol. Soc. Am.*, 96 (4 A): 1512–1522. https://doi.org/10.1785/0120050210.

Boore, D. M. 2010. "Orientation-independent, nongeometric-mean measures of seismic intensity from two horizontal components of motion." *Bull. Seismol. Soc. Am.*, 100 (4): 1830–1835. https://doi.org/10.1785/0120090400.

Bozorgnia, Y., M. M. Hachem, and K. W. Campbell. 2010. "Ground motion prediction equation ('Attenuation Relationship') for inelastic response spectra." *Earthq. Spectra*, 26 (1): 1–23. https://doi.org/10.1193/1.3281182.

Campbell, K. W., and Y. Bozorgnia. 2007. *Campbell-Bozorgnia NGA Ground Motion Relations for the Geometric Mean Horizontal Component of Peak and Spectral Ground Motion Parameters*. Berkeley, California.

Campbell, K. W., and Y. Bozorgnia. 2014. "Campbell-bozorgnia NGA-West2 horizontal ground motion model for active tectonic domains." *NCEE 2014 - 10th U.S. Natl. Conf. Earthq. Eng. Front. Earthq. Eng.*, (January). https://doi.org/10.4231/D3MS3K235.

Heresi, P., H. Dávalos, and E. Miranda. 2018. "Ground motion prediction model for the peak inelastic displacement of single-degree-of-freedom bilinear systems." *Earthq. Spectra*, 34 (3): 1177–1199. https://doi.org/10.1193/061517EQS118M.

Huang, C., K. Tarbali, and C. Galasso. 2020. "A region-specific ground-motion model for inelastic spectral displacement in northern Italy considering spatial correlation properties." *Seismol. Res. Lett.*, 92 (3): 1979–1991. https://doi.org/10.1785/0220200249.

Jayaram, N., and J. W. Baker. 2010. "Considering spatial correlation in mixed-effects regression and the impact on ground-motion models." *Bull. Seismol. Soc. Am.*, 100 (6): 3295–3303. https://doi.org/10.1785/0120090366.

Kaklamanos, J., L. G. Baise, and D. M. Boore. 2011. "Estimating unknown input parameters when implementing the NGA ground-motion prediction equations in engineering practice." *Earthq. Spectra*, 27 (4): 1219–1235. https://doi.org/10.1193/1.3650372.

Luco, N., and C. A. Cornell. 2007. "Structure-specific scalar intensity measures for near-source and ordinary earthquake ground motions." *Earthq. Spectra*, 23 (2): 357–392. https://doi.org/10.1193/1.2723158.

Pinzon, L. A., S. A. Diaz, L. G. Pujades, and Y. F. Vargas. 2021. "An Efficient Method for Considering the Directionality Effect of Earthquakes on Structures." *J. Earthq. Eng.*, 25 (9): 1679–1708. Taylor & Francis. https://doi.org/10.1080/13632469.2019.1597783.

Roy, R., A. Acharjya, A. Roy, A. Santra, and G. Bhattacharya. 2022. "Response of Structures to Bidirectional Seismic Loading: Research Progress and Future Directions." *J. Struct. Eng.*, 148 (7): 1–21. https://doi.org/10.1061/(asce)st.1943-541x.0003358.

Shahi, S. K., and J. W. Baker. 2014. "NGA-West2 Models for Ground Motion Directionality." *Earthq. Spectra*, 30 (3): 1285–1300. https://doi.org/10.1193/040913EQS097M.

Stafford, P. J., T. J. Sullivan, and D. Pennucci. 2016. "Empirical correlation between inelastic and elastic spectral displacement demands." *Earthq. Spectra*, 32 (3): 1419–1448. https://doi.org/10.1193/020515EQS021M.

Tarbali, K. 2017. "Ground Motion Selection for Seismic Response Analysis." PhD dissertation. Christchurch, New Zealand: University of Canterbury.

Tothong, P., and C. A. Cornell. 2006. "An empirical ground-motion attenuation relation for inelastic spectral displacement." *Bull. Seismol. Soc. Am.*, 96 (6): 2146–2164. https://doi.org/10.1785/0120060018.